Bulletin of the Seismological Society of America, Vol. 107, No. 1, pp. 319–333, February 2017, doi: 10.1785/0120150352

Prediction Equations for Ground-Motion Significant Durations Using the NGA-West2 Database

by Wenqi Du and Gang Wang

Abstract Significant duration is an important parameter in seismic risk assessment. In this article, new prediction equations for significant duration parameters are developed using a recently compiled Next Generation Attenuation-West2 (NGA-West2) database. The use of the greatly expanded NGA-West2 database improves the model predictions for small-to-moderate magnitude and far-source earthquake scenarios. The new model has a functional form with only four predictor variables, namely the moment magnitude (M_w), rupture distance (R_{rup}), time-averaged shear-wave velocity in the top 30 m (V_{S30}), and depth to the top of the rupture (Z_{tor}). A magnitude-dependent aleatory variability term is also proposed. The new model can be used to estimate significant durations for earthquake scenarios with moment magnitude M_w from 3 to 7.9 and rupture distance up to 300 km. The proposed model has been systematically compared with some existing prediction models. In addition, empirical correlations between significant durations and spectral accelerations have been studied using the proposed model and the NGA-West2 database.

Introduction

Damage potential of ground motions is usually related to ground-motion amplitude, frequency content, duration, and other cumulative effects. In current seismic-hazard analysis, the duration parameters may not be regarded as equally important as other amplitude and frequency-content parameters, such as peak ground acceleration (PGA) and spectral accelerations (SAs). However, the ground-motion duration, associated with other amplitude parameters, has been regarded as a meaningful indicator in seismic risk assessment, especially in the geotechnical field. For instance, it is well studied that the pore pressure buildup in liquefiable soils is directly related to the number of cycles of the shaking (e.g., Seed and Lee, 1966; Green and Terri, 2005). It is also observed that long-duration ground motions would increase the liquefaction potential of saturated sands (e.g., Idriss and Boulanger, 2006).

The significance of the duration effect on structural response is still controversial. As described by Hancock and Bommer (2006), some researchers found little correlation between duration and peak structural responses (e.g., Iervolino *et al.*, 2006), whereas other researchers observed a positive correlation between duration and cumulative damage measures (e.g., Bommer *et al.*, 2004; Hancock and Bommer 2007). Recently, Chandramohan *et al.* (2016) found that structures with higher deformation capacities and rapid rates of cyclic deterioration would be more susceptible to damage under long-duration ground motions.

As summarized by Bommer and Martinez-Pereira (1999), there have been more than 30 definitions of ground-motion durations in the literature. Among these definitions, significant duration (termed as Ds) is one of the most widely used metrics. Ds can be defined on the basis of the Arias intensity (Arias, 1970), which is given by the following equation:

$$I_A = \frac{\pi}{2g}\int_0^{t_{max}} a(t)^2 dt, \tag{1}$$

in which I_A is the Arias intensity; t_{max} is the total duration of ground-motion time history; and g refers to acceleration of gravity. Significant durations are then evaluated as the time interval over which specified proportions of normalized I_A are accumulated. Two kinds of significant durations are commonly used, namely the time intervals between 5%–75% and 5%–95% of I_A (denoted as Ds_{5-75} and Ds_{5-95}, respectively). Other time intervals such as 20%–80% of I_A have also been used for some applications. Figure 1 shows an example of the computed significant durations using a ground-motion record from the Next Generation Attenuation-West2 (NGA-West2) database (Ancheta *et al.*, 2014). Apparently, Ds_{5-95} is always greater than Ds_{5-75} for a given time history. It is also worth mentioning that a completely different definition of ground-motion duration has been proposed recently, which is based on minimizing the mismatch between the observed response spectrum and the one estimated from the random vibration theory (Bora *et al.*, 2014, 2015).

A number of researchers have proposed prediction equations for different significant duration parameters

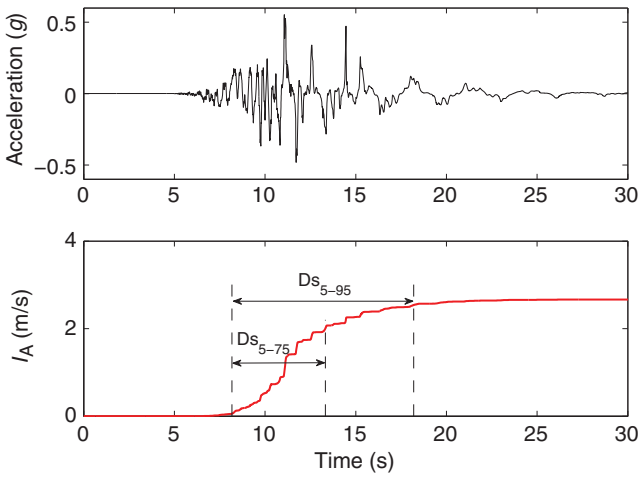

Figure 1. Example of the significant durations $Ds_{5–75}$ and $Ds_{5–95}$ for ground motion recorded at the Botanical Gardens site during the 2011 Christchurch earthquake (east–west direction). The color version of this figure is available only in the electronic edition.

(e.g., Trifunac and Brady, 1975; Abrahamson and Silva, 1996; Hernandez and Cotton, 2000; Kempton and Stewart, 2006; Bommer *et al.*, 2009; Lee and Green, 2014; Yaghmaei-Sabegh *et al.*, 2014; Ghofrani and Atkinson, 2015; Afshari and Stewart, 2016). The detailed information of these prediction equations is summarized in Table 1, where various ground-motion database and predictor variables were employed. Although there are dozens of existing prediction equations, the number of globally applicable models is still limited: two models (Kempton and Stewart, 2006; Bommer *et al.*, 2009) were developed using subsets of the NGA phase 1 database (NGA-West1; Chiou *et al.*, 2008), and one recent model (Afshari and Stewart, 2016) was developed using the NGA-West2 database (Ancheta *et al.*, 2014). Because the NGA-West2 database consisting of 21,335 ground-motion records from a variety of worldwide earthquakes has been compiled recently, it is necessary to further explore the features of Ds based on the expanded database.

The objective of this article is to develop prediction equations for significant durations ($Ds_{5–75}$ and $Ds_{5–95}$) using the latest NGA-West2 ground-motion database. Simple functional form employing four predictor variables is proposed based on a mixed-effects regression analysis. Then, the performance of the proposed equations is compared with some existing models. Finally, empirical correlation between the residuals of Ds and SA, which is required to predict the joint distribution of multiple intensity measures (IMs), is also studied using the expanded database.

Ground-Motion Database

In this article, a subset of the Pacific Earthquake Engineering Research Center's (PEER) NGA-West2 database (Ancheta *et al.*, 2014) is selected to develop the empirical models for significant duration (Ds) of ground motions. The NGA-West2 database includes a total of over 21,000 three-component uniformly processed recordings, most of which were recorded in free fields. They have been used to develop the latest NGA-West2 ground-motion prediction equations (GMPEs) for shallow crustal earthquakes in active tectonic regions (Abrahamson *et al.*, 2014; Boore *et al.*, 2014; Campbell and Bozorgnia, 2014; Chiou and Youngs, 2014).

The exclusion criteria introduced by Campbell and Bozorgnia (2014) are adopted herein to select the reliable records. The criteria goal at excluding low-quality, unreliable, incomplete or poorly recorded data, aftershocks,

Table 1
Summary of the Prediction Equations for Various Significant Durations

Duration Parameter	Predictors	Regions of Records	Number of Earthquakes Used	Number of Records Used	Reference
$Ds_{5–95}$	M, R_{epi}, S	United States	49	188	Trifunac and Brady (1975)
$Ds_{5–75}$, $Ds_{5–95}$	M_w, R_{rup}, S	–	–	–	Abrahamson and Silva (1996)
$Ds_{5–95}$	M_s, R_{rup}, S	California and Italy	32	272	Hernandez and Cotton (2000)
$Ds_{2.5–97.5}$	M, R_{rup}, Ts	Mexico	12	> 800	Reinoso and Ordaz (2001)
$Ds_{5–75}$, $Ds_{5–95}$	M_w, R_{rup}, $Z_{1.5}$, V_{S30},	Global	73	1559	Kempton and Stewart (2006, referred to as KS06)
$Ds_{5–75}$, $Ds_{5–95}$	M_w, R_{rup}, V_{S30}, Z_{tor}	Global	114	2406	Bommer *et al.* (2009, referred to as BSA09)
$Ds_{5–75}$, $Ds_{5–95}$	M_w, R_{rup}, S	Stable continental	4	28	Lee and Green (2014)
$Ds_{5–75}$, $Ds_{5–95}$	M_w, R_{rup}, S	Iran	141	286	Yaghmaei-Sabegh *et al.* (2014)
$Ds_{5–75}$, $Ds_{5–95}$	R_{rup}, V_{S30}	Japan	Tohoku earthquake (2011)	1735	Ghofrani and Atkinson (2015)
$Ds_{20–80}$, $Ds_{5–75}$, $Ds_{5–95}$	M_w, R_{rup}, V_{S30}, Z_1	Global	–	11,195	Afshari and Stewart (2016)
$Ds_{5–75}$, $Ds_{5–95}$	M_w, R_{rup}, V_{S30}, Z_{tor}	Global	311	13,958	This study

M, earthquake magnitude; M_s, surface-wave magnitude; M_w, moment magnitude; R_{epi}, epicentral distance (km); R_{rup}, closest distance from site to the rupture plane (km); S, indicator of soil types; Ts, fundamental site period (s); V_{S30}, average shear-wave velocity of the upper 30 m (m/s); Z_{tor}, depth to the top of rupture (km); Z_1, depth from the ground surface to the 1 km/s shear-wave surface (km); $Z_{1.5}$, depth from the ground surface to the 1.5 km/s shear-wave surface (km).

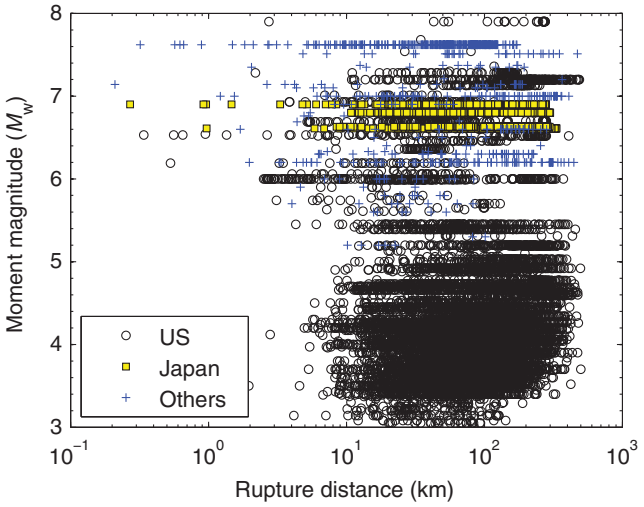

Figure 2. Distribution of earthquake recordings used in this study. The color version of this figure is available only in the electronic edition.

non-free-field recordings, non-shallow-crustal earthquakes, and data with only one horizontal component. The detailed criteria have been listed in Campbell and Bozorgnia (2013). In addition, visual inspection indicates that some low-amplitude and long-duration acceleration-time histories seem to be affected by signal noise. Inclusion of these ground motions may not influence the predictions of amplitude-based IMs (e.g., NGA-West2 GMPEs), but they do influence the predictions of duration parameters. Thus, the exclusion criteria used by Afshari and Stewart (2016), which are based on comparing the durations estimated from the acceleration and velocity-time histories, are used to further exclude these noisy, unreasonable recordings from the database. The final selected database is composed of 13,958 recordings from 311 earthquakes with moment magnitudes M_w from 3.05 to 7.9 and rupture distances (closest distance from the site to the ruptured area) R_{rup} ranging from 0.1 to 499.54 km. The moment magnitude and rupture distance distribution of records contained in the database is shown in Figure 2. The NGA-West2 flatfile containing detailed information of these ground motions was also downloaded from the PEER website (see Data and Resources).

Regression Analysis

A typical ground-motion duration model for the mixed-effects regression analysis takes the form as

$$\ln(\mathrm{Ds_{GM}})_{ij} = \overline{\ln(\mathrm{Ds_{GM}})_{ij}} + \eta_i + \varepsilon_{ij}, \tag{2}$$

in which $\ln(\mathrm{Ds_{GM}})$ and $\overline{\ln(\mathrm{Ds_{GM}})}$ denote the logarithm of measured and predicted geometric mean of significant durations ($\mathrm{Ds_{5–75}}$ or $\mathrm{Ds_{5–95}}$) from two as-recorded horizontal components; i and j denote the jth recording in the ith event, respectively. η_i and ε_{ij} represent the between-event residuals and within-event residuals, which are assumed to be normally distributed with zero means and standard deviations τ and ϕ, respectively (Abrahamson and Youngs, 1992). The advantage of the mixed-effects model is that it can separate the total residuals into two components: between-event and within-event. Therefore, it has been widely used to develop GMPEs in earthquake engineering (e.g., Foulser-Piggott and Stafford, 2012; Du and Wang, 2013; Campbell and Bozorgnia, 2014).

It has been studied that many engineering applications need an estimate of the arbitrary horizontal component of IMs (Baker and Cornell, 2006). For an arbitrary horizontal component of the measured Ds, the component-to-component residuals can be computed as

$$\xi_{ijk} = \ln \mathrm{Ds}_{ijk} - \ln(\mathrm{Ds_{GM}})_{ij}, \tag{3}$$

in which Ds_{ijk} is the measured Ds for the kth ($k = 1,2$) horizontal component of the jth recording and the ith event; ξ_{ijk} denotes the component-to-component residuals of the two horizontal components with an assumed zero mean and a standard deviation of ϕ_c. ϕ_c can be calculated by the following equation:

$$\phi_c^2 = \frac{1}{4N}\sum_{l=1}^{N}(\ln \mathrm{Ds}_{l1} - \ln \mathrm{Ds}_{l2})^2 \tag{4}$$

(Boore, 2005), in which subscripts 1 and 2 denote the two horizontal components of the measured Ds; l is the recording number index; and N is the total number of recordings in the database.

Therefore, the total standard deviation (σ) for the geometric mean component and the total standard deviation (σ_{ARB}) for the arbitrary horizontal component of Ds can be determined as follows:

$$\sigma = \sqrt{\phi^2 + \tau^2} \tag{5}$$

$$\sigma_{\mathrm{ARB}} = \sqrt{\phi^2 + \tau^2 + \phi_c^2}. \tag{6}$$

The symbols ϕ, τ, and σ are consistent with the notations suggested by Al Atik *et al.* (2010).

The mixed-effect regression analysis is conducted using the nlme package in the statistical programming software R (Pinheiro *et al.*, 2008). The algorithm is similar to that proposed by Abrahamson and Youngs (1992). The regressed coefficients, between-event and within-event residuals, as well as the values of standard statistical metrics can be obtained by performing the nlme model in one stage.

Functional Form

To develop an appropriate functional form, the existing prediction equations for Ds can provide some useful insights. The significant duration at the source is usually assumed to be equivalent to the source duration D_{source}. For significant duration at a given site, the effects of traveling paths, site

conditions, and other seismological conditions need to be well accounted for. Magnitude scaling of the source duration has been studied based on seismological considerations (Abrahamson and Silva, 1996; Kempton and Stewart, 2006). As suggested by theoretical seismic source models (e.g., Boore, 1983), D_{source} is inversely related to the corner frequency f_c in the Fourier amplitude spectrum of the ground motion. Such corner frequency f_c has been related to the seismic moment (Brune, 1970). Therefore, the source duration D_{source} can be expressed as follows:

$$D_{\text{source}} = \frac{1}{f_c} = \frac{1}{4.9 \times 10^6 \times \beta} \left(\frac{M_0}{\Delta\sigma}\right)^{1/3}, \tag{7}$$

in which β is the crustal shear-wave velocity at the source (km/s), $\Delta\sigma$ is the stress-drop index (bars), and M_0 denotes the seismic moment (dyn·cm). Assuming that $\Delta\sigma$ and M_0 are related to the moment magnitude M_{w} through the following relationships: $\Delta\sigma = \exp(b_1 + b_2(M_{\text{w}} - 6))$ and $M_0 = 10^{1.5M_{\text{w}}+16.05}$; Bommer *et al.* (2009) recast equation (7) into an equivalent, but simpler, linear functional form as $\ln D_{\text{source}} = c_0 + m_1 M_{\text{w}}$, in which c_0 and m_1 are parameters to be determined by regression analysis. Other functional forms for the magnitude scaling have also been proposed, for example, a power M_{w} function (Yaghmaei-Sabegh *et al.*, 2014) based on the regression of strong-motion data in Iran.

Although the linear magnitude scaling of the logarithmic source duration is based on physical considerations, the functional form was only applied to moderate-to-large earthquakes in previous studies. For example, the Kempton and Stewart (2006) model is valid for $5 \le M_{\text{w}} \le 7.6$ and $R_{\text{rup}} \le 200$ km, whereas the model proposed by Bommer *et al.* (2009) is applicable for $4.8 \le M_{\text{w}} \le 7.9$ and for R_{rup} up to 100 km. Figure 3 shows the distributions of the empirical $\text{Ds}_{5\text{–}75}$ and $\text{Ds}_{5\text{–}95}$ calculated from the selected NGA-West2 database, together with linear regression lines showing the trend of the data versus moment magnitude in various R_{rup} bins. The data can be clearly separated into two groups. A linear increase of significant durations with increasing M_{w} is evident for moderate-to-large events ($M_{\text{w}} \ge 5.3$) at R_{rup} up to around 100 km. However, the significant durations are almost independent of M_{w} for relatively small events ($M_{\text{w}} < 5.3$). Observation of the near-source duration data in Figure 3 ($R_{\text{rup}} = 0$–10 km) further implies that the source durations for small events ($M_{\text{w}} < 5.3$) are approximately M_{w} independent. Direct extrapolation of linear magnitude scaling based on the moderate-to-large events would significantly underestimate durations in the small-magnitude range. In addition, the significant durations are not notably affected by moment magnitudes at far distances (150 km $\le R_{\text{rup}} \le$ 300 km). The above observations are also supported by several recent studies on ground-motion durations using the NGA-West2 database (e.g., Boore and Thompson, 2014; Afshari and Stewart, 2016).

There are several possibilities to reconcile the notable difference in the magnitude scaling of durations between small and moderate-to-large earthquake events. To cast the source duration into the theoretical expression shown in equation (7), different magnitude-dependent $\Delta\sigma$ terms are needed for small and moderate-to-large events, as proposed in Afshari and Stewart (2016). However, it is worth mentioning that the $\Delta\sigma$ term is just a stress-drop index, not the true stress drop (e.g., Allmann and Shearer, 2009). One would rather regard it as an unknown parameter that needs to be backcalculated from the empirical data. Another possible explanation is that, the $D_{\text{source}} \sim f_c^{-1}$ relationship in equation (7) is mainly based on the observational and theoretical expectations of moderate-to-large ground motions (e.g., Hanks and McGuire, 1981; Boore, 1983). For small-magnitude events, the source duration may not be well correlated with f_c^{-1}.

Several functional forms for the magnitude scaling were tried and tested to fit the trend of empirical data. Standard statistical metrics such as the Akaike information criterion, the Bayesian information criterion, and the log-likelihood tests were used to compare the different scaling terms. The results showed that the piecewise linear magnitude-scaling function performed better than the other magnitude scaling forms. Similar statistical tests were also performed for the scaling of other parameters, such as rupture distance, site condition, and fault category. After extensive trials and comparisons, the final functional expression is proposed:

$$\ln(\text{Ds}) = c_1 + f_{M,R} + c_6 \times \ln(V_{S30}) + c_7 \times Z_{\text{tor}}, \tag{8}$$

in which ln(Ds) denotes the natural log of signification duration ($\text{Ds}_{5\text{–}75}$ or $\text{Ds}_{5\text{–}95}$); V_{S30} represents the time-averaged shear-wave velocity of the upper 30 m (m/s); Z_{tor} is the depth to the top of the fault rupture (km); $f_{M,R}$ represents the piecewise magnitude- and rupture distance-dependent function as follows:

$$f_{M,R} = \begin{cases} c_2 \times \ln\left(\sqrt{R_S^2 + h^2}\right) + c_3 \times \ln\left(\frac{R_F}{150}\right); & \text{for } M_{\text{w}} < 5.3 \\ c_2 \times \ln\left(\sqrt{R_S^2 + h^2}\right) + c_3 \times \ln\left(\frac{R_F}{150}\right) + c_4 \times (M_{\text{w}} - 5.3)\left[1 - \frac{\ln\left(\sqrt{R_S^2 + h^2}\right)}{\ln\left(\sqrt{150^2 + h^2}\right)}\right]; & \text{for } 5.3 \le M_{\text{w}} < 7.5 \\ c_2 \times \ln\left(\sqrt{R_S^2 + h^2}\right) + c_3 \times \ln\left(\frac{R_F}{150}\right) + c_4 \times (M_{\text{w}} - 5.3)\left[1 - \frac{\ln\left(\sqrt{R_S^2 + h^2}\right)}{\ln\left(\sqrt{150^2 + h^2}\right)}\right] + c_5 (M_{\text{w}} - 7.5) \times \ln\left(\frac{R_F}{150}\right); & \text{for } M_{\text{w}} \ge 7.5 \end{cases}, \tag{9}$$

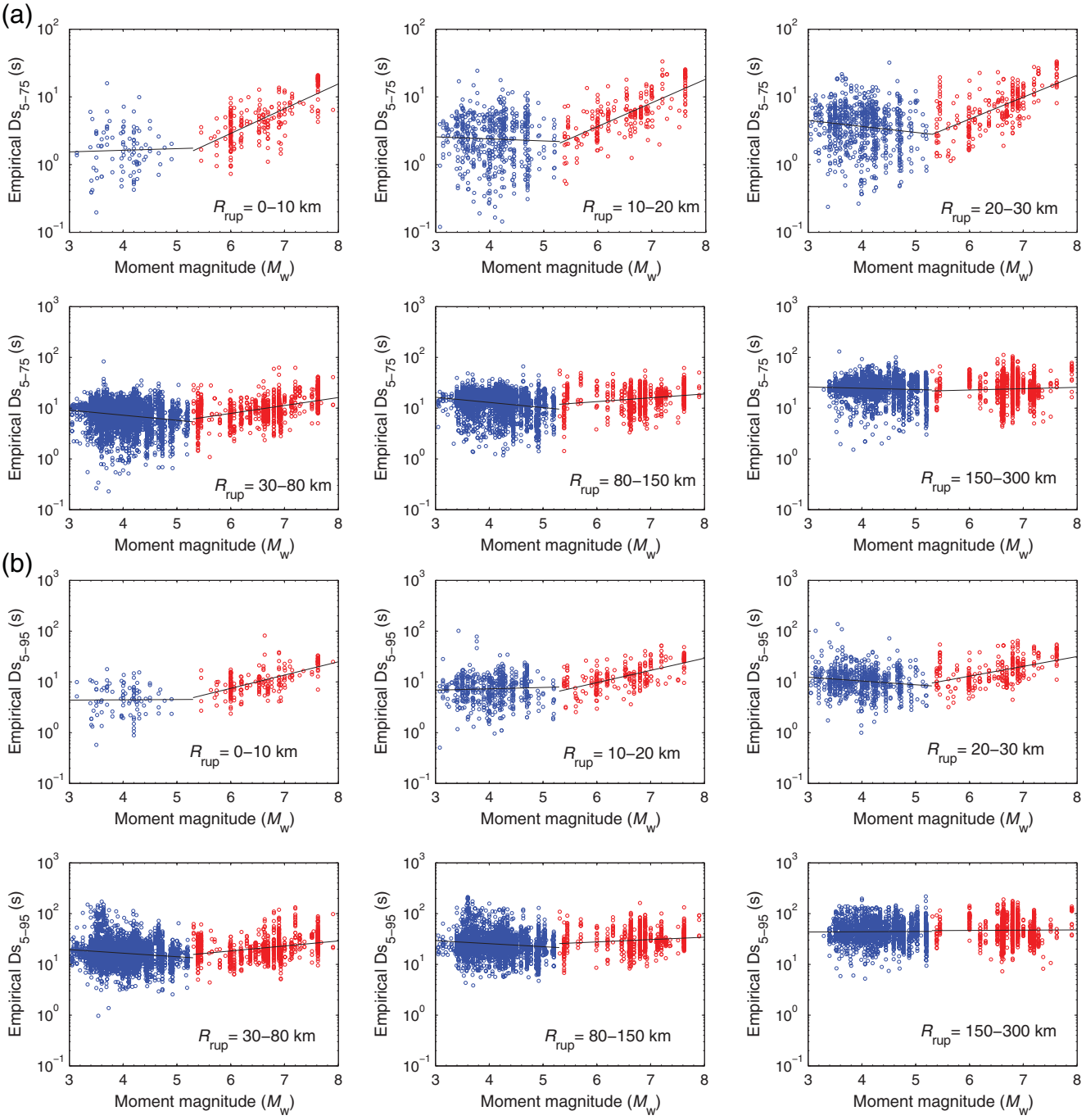

Figure 3. Distributions of significant durations versus moment magnitudes: (a) $Ds_{5–75}$ and (b) $Ds_{5–95}$ for various R_{rup} bins. The solid lines are obtained by simple linear regression. The color version of this figure is available only in the electronic edition.

in which M_w refers to the moment magnitude; R_S and R_F are two distance parameters defined as $R_S = \min(R_{rup}, 150)$ and $R_F = \max(R_{rup}, 150)$ in kilometers, in which R_{rup} stands for the rupture distance (km); and h is a fictitious hypocentral depth (km). According to the above definition, R_S equals to R_{rup} when R_{rup} is smaller than 150 km, controlling the short-to-moderate distance scaling. R_F equals to R_{rup} if R_{rup} is greater than 150 km, controlling the long-distance scaling. Inclusion of R_S and R_F in the functional form can better fit empirical data in terms of the distance scaling.

The new model employs a piecewise magnitude-scaling function delineated by M_w 5.3 and 7.5, which is motivated by the empirical data in Figure 3. For small-magnitude events ($M_w < 5.3$), the predictive model is independent of M_w. For moderate-to-large magnitude events ($M_w \geq 5.3$), the magnitude scaling is influenced by the rupture distance

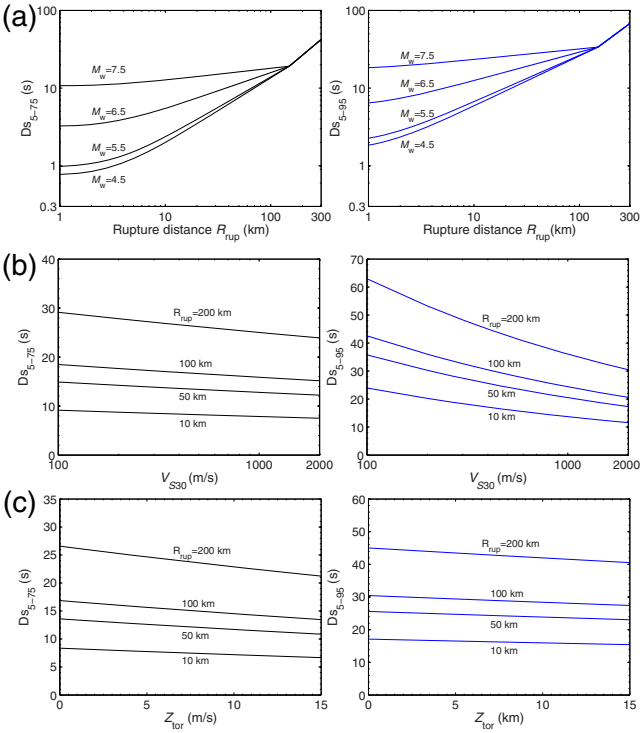

Figure 4. Median predicted Ds_{5-75} and Ds_{5-95} with respect to R_{rup}, M_w, V_{S30}, and Z_{tor}, respectively. The values of other predictor variables in these plots are (a) $V_{S30} = 400$ m/s and $Z_{tor} = 0$ km; (b) $M_w = 7$ and $Z_{tor} = 0$ km; (c) $M_w = 7$ and $V_{S30} = 400$ m/s. The color version of this figure is available only in the electronic edition.

through a multiplier $[1 - \frac{\ln(\sqrt{R_S^2+h^2})}{\ln(\sqrt{150^2+h^2})}]$, which decreases from a positive value to zero when R_{rup} increases from 0 to 150 km. The multiplier becomes zero if $R_{rup} \geq 150$ km, indicating that the significant durations are not notably affected by moment magnitudes at far distances, as discussed before.

The model coefficients as well as the associated 95% confidence intervals for Ds_{5-75} and Ds_{5-95} are shown in Table 2. All coefficients yield very small p-values, so they are statistically significant. It is worth noting that some other ground-motion parameters such as the fault type and sediment depth were also tried and tested in this process, but they were removed from the final functional form due to statistical insignificance.

The proposed model would be valid for shallow crustal earthquakes with M_w between 3 and 7.9, R_{rup} ranging from 0 to 300 km, and V_{S30} values in the 80–2100 m/s range. Figure 4 shows the median predicted values of Ds_{5-75} and Ds_{5-95} with respect to M_w, R_{rup}, V_{S30}, and Z_{tor}, respectively. It is clearly shown that both the Ds_{5-75} and Ds_{5-95} are strongly dependent on the magnitude and distance scalings, whereas the influence of V_{S30} and Z_{tor} is relatively weak. Figure 4a shows that Ds is dependent on M_w only at short-to-moderate distance range ($R_{rup} \leq 150$ km). The significant durations greatly increase with increasing M_w for moderate-to-large events ($M_w \geq 5.5$), which is physically expected because these events are generally associated with large fault dimension and long rupture duration at the sources (Dobry *et al.*, 1978). The notable increase of duration at far distances is mainly caused by the increasing refractions and reflections of body waves over the travel path as well as the arrival of slowly propagating surface waves. Besides, the slight increase of durations at soft soil sites (smaller V_{S30}) is mainly due to resonance effects within soil layers. Longer duration would also be expected for smaller Z_{tor} values, possibly due to the fact that the depth of buried ruptures can influence the stress drop $\Delta\sigma$ in the fault rupture process (Kagawa *et al.*, 2004). These observations are generally consistent with previous studies (e.g., Bommer *et al.*, 2009).

Aleatory Variability Model

The between-event and within-event residuals of the regression models for Ds_{5-75} and Ds_{5-95} are plotted versus M_w, R_{rup}, V_{S30}, and Z_{tor} in Figures 5 and 6, respectively. In these plots, the residuals are obtained by the nlme package in *R*. The between-event and within-event residuals are then partitioned into 10 nonoverlapping M_w bins with an increment of 0.5, and 10 nonoverlapping Z_{tor} bins of 2 km in size. The within-event residuals are also partitioned into nine bins equally spaced with respect to $\ln(R_{rup})$ and $\ln(V_{S30})$ values, respectively. The black square symbols indicate the local means of these binned residuals, and their 95% confidence intervals are shown as dashed lines. It can be observed that there is a slightly biased trend for the between-event residuals of Ds_{5-75} at the small magnitude range, which is caused by reinforcing the M_w-independent functional form for small-magnitude events. No clear biases or trends with respect to

Table 2
Regression Coefficients of the Proposed Significant Duration Model

	Ds_{5-75}			Ds_{5-95}		
Coefficient	Mean Value	95% Confidence Interval		Mean Value	95% Confidence Interval	
c_1	−0.912	−1.073	−0.750	1.736	1.597	1.875
c_2	0.850	0.831	0.869	0.645	0.630	0.662
c_3	1.142	1.091	1.192	1.005	0.961	1.049
c_4	1.587	1.506	1.668	1.161	1.091	1.231
c_5	1.726	0.114	3.338	1.231	0.204	2.662
c_6	−0.066	−0.089	−0.044	−0.242	−0.262	−2.224
c_7	−0.015	−0.023	−0.007	−0.007	−0.014	0.000
h	3.296	1.986	4.606	1.318	0.159	2.478

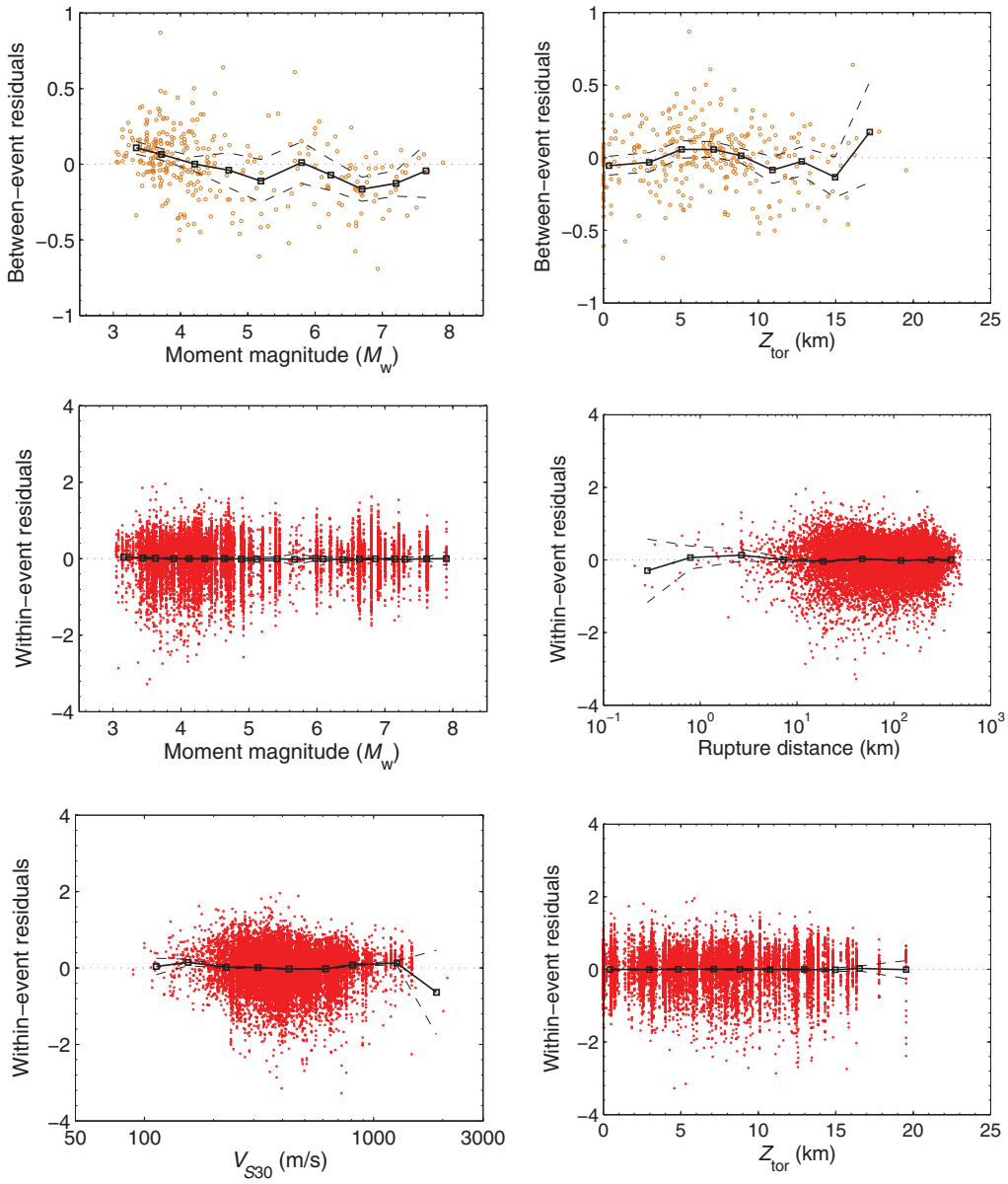

Figure 5. Distributions of the between-event and within-event residuals with respect to M_w, Z_{tor}, and within-event residuals with respect to R_{rup} and V_{S30} for the significant duration $Ds_{5–75}$. The black square denotes the local mean value of each binned residuals, and the dashed curves denote their 95% confidence intervals. The color version of this figure is available only in the electronic edition.

these predictor variables can be observed in other plots. The few slightly biased points (e.g., V_{S30} as 2000 m/s) are possibly caused by a paucity of data. The distributions of the residuals imply that the selected functional form can provide generally unbiased predictions for the significant durations.

As mentioned previously, the standard deviations of the between-event variability, within-event variability, and component-to-component variability are expressed as τ, ϕ, and ϕ_c, respectively. The within-event residuals show a strong magnitude-dependent distribution; the variability of the residuals is notably larger for smaller magnitude ($M_w < 5$), as shown in Figure 7a. The component-to-component residuals were also found to be magnitude dependent (shown in Fig. 7c). Therefore, it would be desirable to empirically develop a magnitude-dependent aleatory variability model. The two kinds of residuals were first partitioned into several overlapping magnitude bins with 0.5-unit M_w width. The standard deviation of within-event residuals in each bin can then be calculated using the maximum-likelihood method adopted in the Abrahamson and Youngs (1992) algorithm, whereas the component-to-component standard deviation of residuals in each bin can be computed via equation (4). Figure 7b and 7d shows the distributions of the computed standard deviations of the within-event and component-to-component residuals within varying magnitude bins, respectively. Thus, the standard deviations ϕ and ϕ_c can be estimated by the following trilinear magnitude-dependent equations:

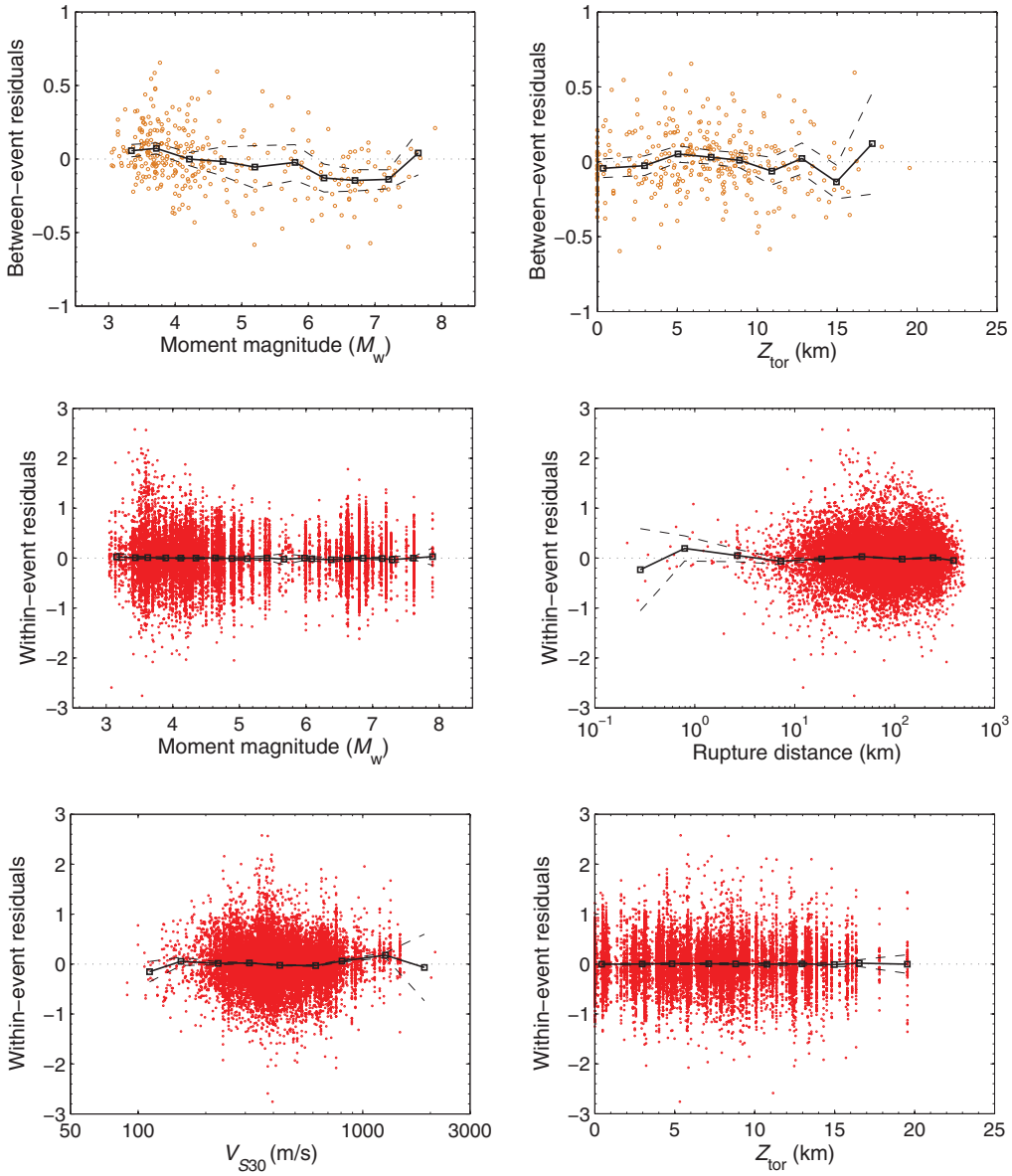

Figure 6. Distributions of the between-event and within-event residuals with respect to M_w, Z_{tor}, and within-event residuals with respect to R_{rup} and V_{S30} for the significant duration Ds_{5-95}. The black square denotes the local mean value of each binned residuals, and the dashed curves denote their 95% confidence intervals. The color version of this figure is available only in the electronic edition.

$$\phi = \begin{cases} \phi_1 & M_w \leq 5 \\ \phi_2 + 2(\phi_1 - \phi_2) \times (5.5 - M_w) & 5 < M_w < 5.5 \\ \phi_2 & M_w \geq 5.5 \end{cases} \tag{10}$$

$$\phi_c = \begin{cases} \phi_{c1} & M_w \leq 5 \\ \phi_{c2} + 2(\phi_{c1} - \phi_{c2}) \times (5.5 - M_w) & 5 < M_w < 5.5 \\ \phi_{c2} & M_w \geq 5.5 \end{cases}, \tag{11}$$

in which ϕ_i and ϕ_{ci} ($i = 1,2$) are regressed parameters. The proposed trilinear variability models of the within-event and component-to-component residuals for Ds_{5-75} are shown (solid lines) in Figure 7b and 7d, respectively. It is seen that the trilinear curves generally fit the empirical points well. The distribution of the between-event residuals does not show such dependency, and therefore, the constant value τ obtained by regression analysis can be directly used for various earthquake scenarios.

Table 3 presents the values of τ, ϕ_i, and ϕ_{ci} ($i = 1, 2$) obtained from the above analysis. The total standard deviations for geometric mean component (σ) and arbitrary horizontal component (σ_{ARB}) can then be calculated by equations (5) and (6), respectively. The values of σ and σ_{ARB} for specific scenarios are also listed in Table 3.

Figure 8 shows the median and median $\pm$ 1 standard deviation predicted Ds_{5-75} and Ds_{5-95} for a variety of earthquake scenarios associated with the empirical data in the present database. For a given earthquake scenario with input

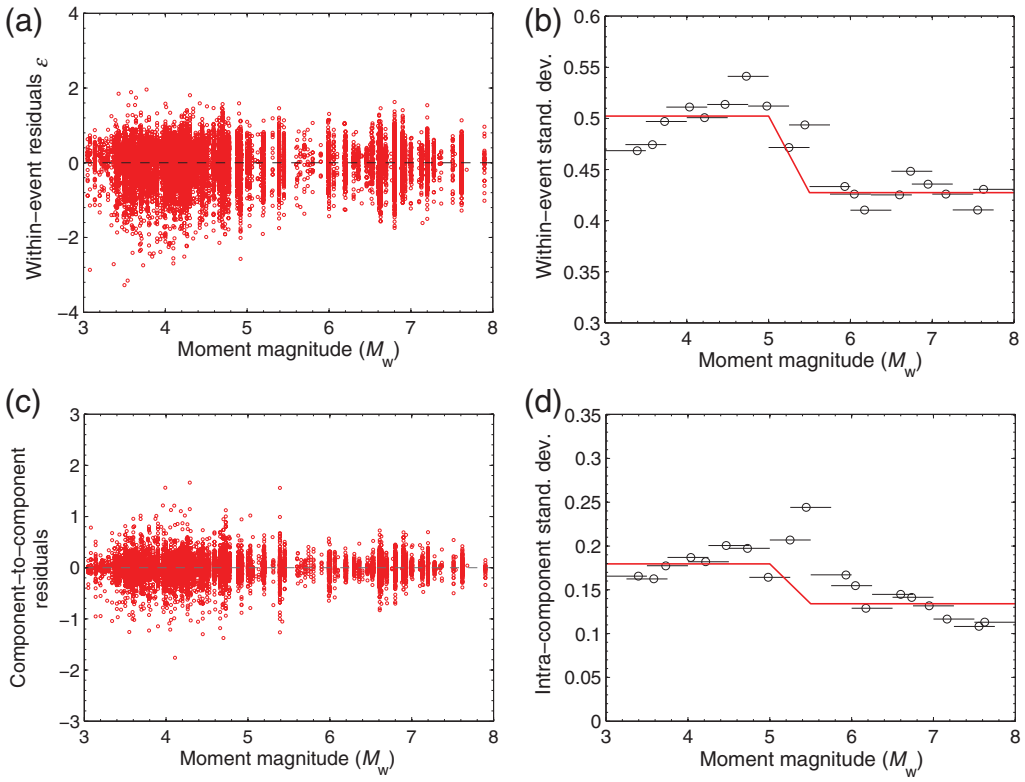

Figure 7. (a) Distribution of the within-event residuals for $Ds_{5–95}$ versus M_w; (b) within-event standard deviations for overlapping magnitude bins and the proposed trilinear variability model (equation 10); (c) distribution of the component-to-component residuals for $Ds_{5–95}$ versus M_w; and (d) component-to-component standard deviations and the proposed trilinear variability model (equation 11). It is noted that the horizontal bar in (b) and (d) indicates the interval of the magnitude bin. The color version of this figure is available only in the electronic edition.

parameters [M_w, Z_{tor}, V_{S30}], the empirical data are selected based on a combination of magnitude bin [$M_w - 0.25$, $M_w + 0.25$], depth to the top of rupture bin [$Z_{tor} - 2$ km, $Z_{tor} + 2$ km], and shear-wave velocity bin [$V_{S30} - 100$ m/s, $V_{S30} + 100$ m/s]. It appears that the estimates of $Ds_{5–75}$ and $Ds_{5–95}$ are generally in agreement with the empirical data, and then the proposed model can broadly capture the scaling of significant durations versus rupture distances.

Comparison with Other Models

In this section, the performance of the new model is compared with several previous studies. Three global models from Table 1 are selected (Kempton and Stewart, 2006, hereafter, KS06; Bommer *et al.*, 2009, hereafter BSA09; Afshari and Stewart, 2016, hereafter AS16). As mentioned previously, these three models were developed using the NGA-West1 or NGA-West2 strong-motion database. Some predictor variables such as M_w, R_{rup}, and V_{S30} are commonly used in these models. Therefore, they are appropriate to perform direct comparisons with the new model. It should be noted that for the KS06 model, only the base model without the consideration of basin or directivity effect is used herein.

Distance scalings of the median predictions of $Ds_{5–75}$ and $Ds_{5–95}$ are compared in Figure 9. The predictions are evaluated for a strike-slip earthquake with $V_{S30} = 400$ m/s,

Table 3
Coefficients of the Proposed Variability Model in Equations (10) and (11)

						$M_w \le 5$		$M_w \ge 5.5$	
Duration Parameter	τ	ϕ_1	ϕ_2	ϕ_{c1}	ϕ_{c2}	σ	σ_{ARB}	σ	σ_{ARB}
$Ds_{5–75}$	0.247	0.502	0.427	0.180	0.134	0.559	0.588	0.493	0.511
$Ds_{5–95}$	0.230	0.437	0.356	0.129	0.123	0.494	0.510	0.424	0.441

τ, standard deviation of between-event residuals; ϕ_1, ϕ_2, parameters to estimate the standard deviation of within-event residuals (ϕ); ϕ_{c1}, ϕ_{c2}, parameters to estimate the component-to-component standard deviation (ϕ_c); σ, standard deviation of the total residuals for the geometric mean duration ($\sigma = \sqrt{\phi^2 + \tau^2}$); σ_{ARB}, standard deviation of the total residuals for the arbitrary horizontal component ($\sigma_{ARB} = \sqrt{\sigma^2 + \phi_c^2}$). σ and σ_{ARB} for $5 < M_w < 5.5$ linearly interpolate the values for M_w 5 and 5.5.

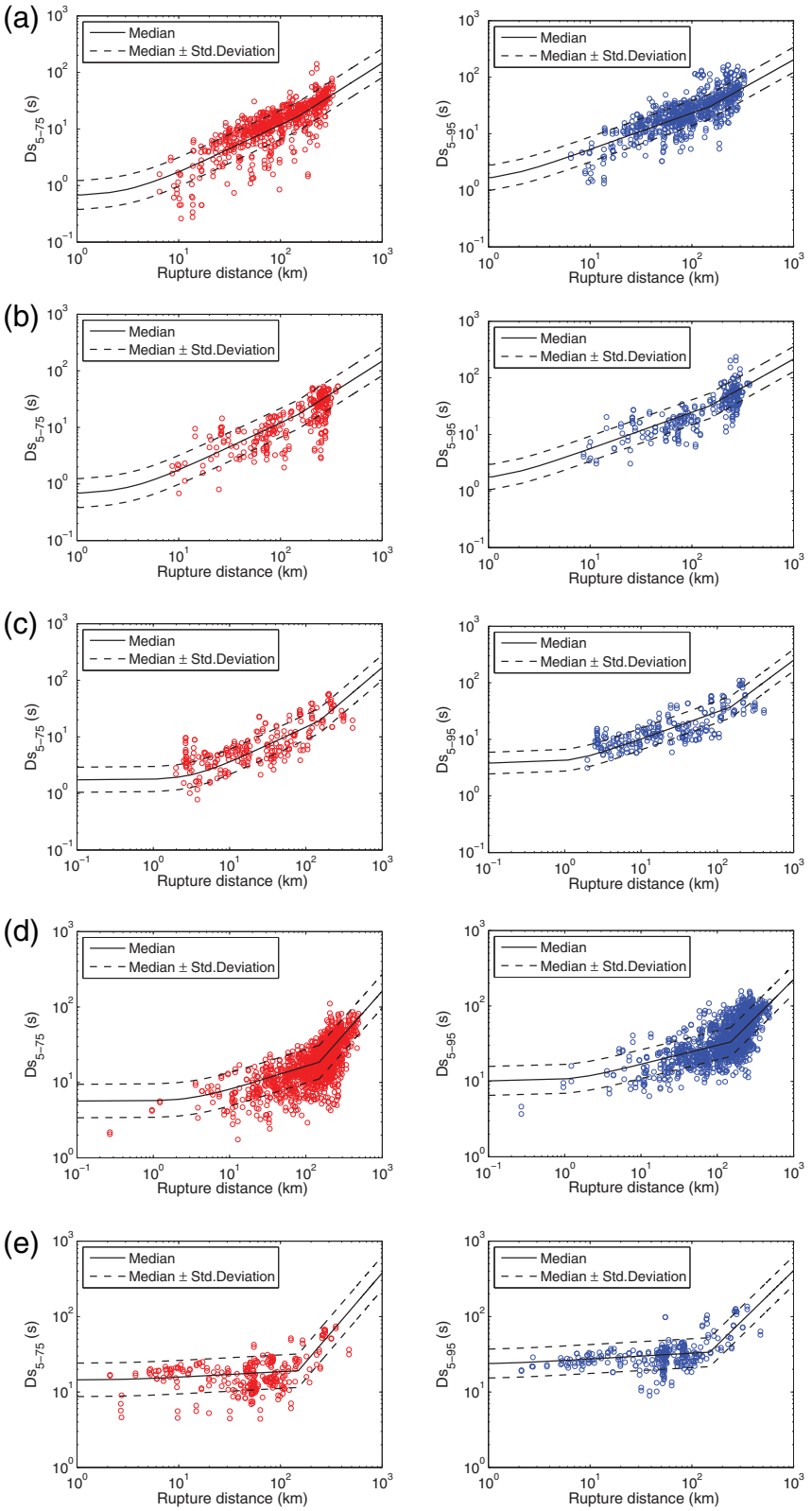

Figure 8. Comparisons of the predicted M_w and M_w against empirical data for five earthquake scenarios: (a) $M_w = 4$, $Z_{tor} = 8$ km, $V_{S30} = 500$ m/s; (b) $M_w = 5$, $Z_{tor} = 8$ km, $V_{S30} = 400$ m/s; (c) $M_w = 6$, $Z_{tor} = 2$ km, $V_{S30} = 250$ m/s; (d) $M_w = 7$, $Z_{tor} = 2$ km, $V_{S30} = 400$ m/s; and (e) $M_w = 7.75$, $Z_{tor} = 0$ km, $V_{S30} = 400$ m/s. The empirical data are selected following a combination of $[M_w - 0.25, M_w + 0.25]$, $[Z_{tor} - 2$ km$, Z_{tor} + 2$ km$]$, and $[V_{S30} - 100$ m/s$, V_{S30} + 100$ m/s$]$. The color version of this figure is available only in the electronic edition.

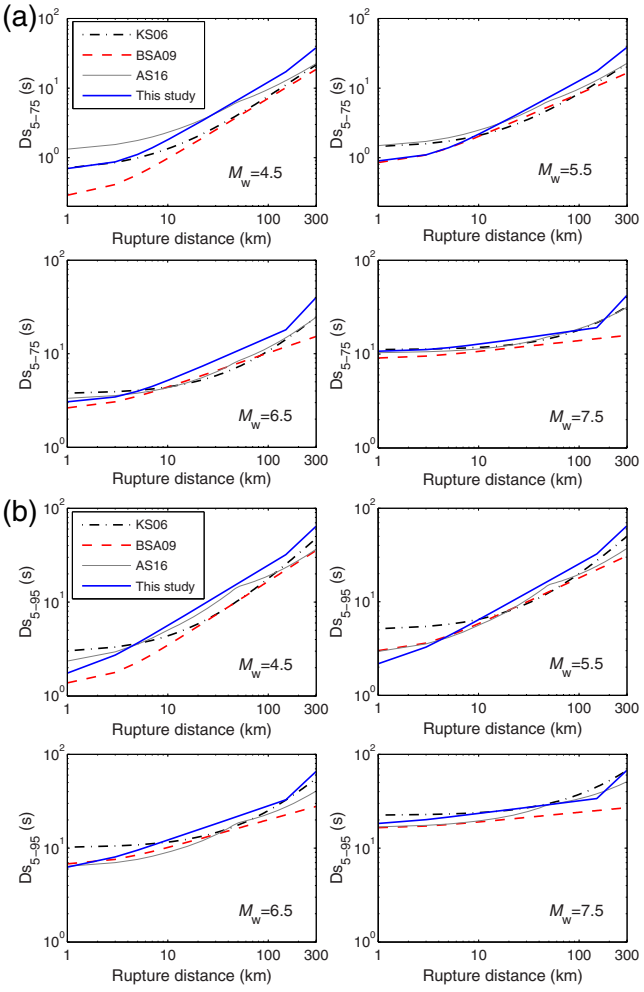

Figure 9. Comparisons of the median predictions of the proposed model with other models versus rupture distance for (a) Ds_{5-75} and (b) Ds_{5-95}. Significant durations are predicted for a strike-slip earthquake and input parameters as V_{S30} = 400 m/s, Z_1 = 0.3 km, and Z_{tor} = 7, 6, 4, and 0 km for M_w = 4.5, 5.5, 6.5, and 7.5, respectively. The color version of this figure is available only in the electronic edition.

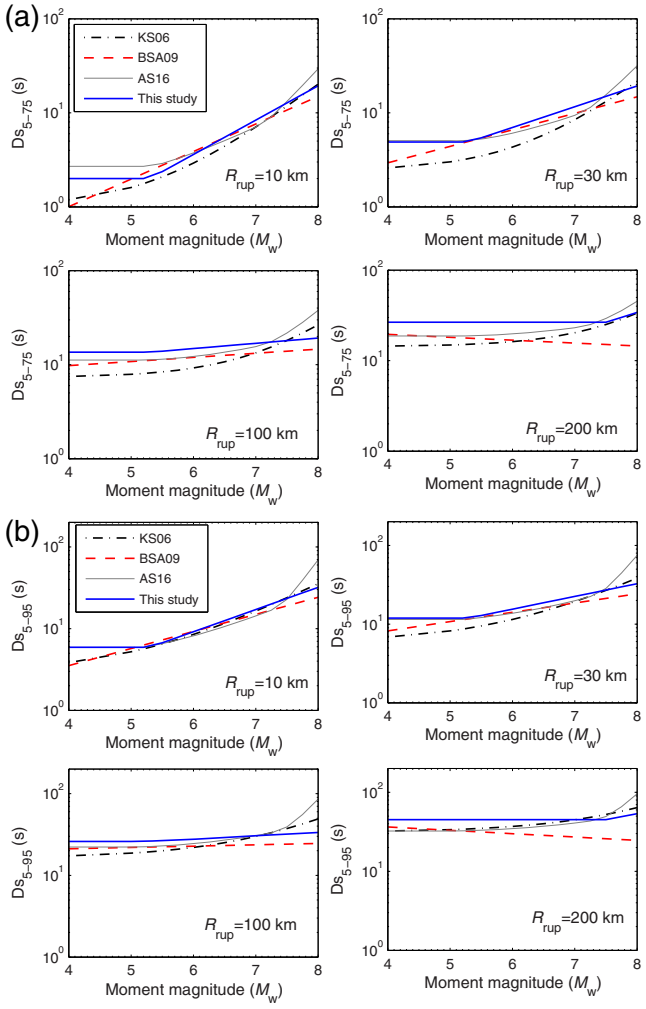

Figure 10. Comparisons of the median predictions of the proposed model with other models versus moment magnitude for (a) Ds_{5-75} and (b) Ds_{5-95}. The other parameters used are V_{S30} = 400 m/s; Z_{tor} = 0 km; and Z_1 = 0.6 km. The color version of this figure is available only in the electronic edition.

Z_1 = 0.3 km, and Z_{tor} as 7, 6, 4, and 0 km for M_w = 4.5, 5.5, 6.5, and 7.5, respectively. These input parameters are generally in line with the estimates provided by Kaklamanos *et al.* (2011). Figure 10 shows the comparisons of magnitude scaling of the median Ds_{5-75} and Ds_{5-95} for R_{rup} as 10, 30, 100, and 200 km, respectively. Other parameters are used as V_{S30} = 400 m/s, Z_{tor} = 0 km, and Z_1 = 0.6 km.

Figures 9 and 10 show predictions by this study are generally consistent with other models, whereas some discrepancies can be observed at short distances (0–10 km) and far distances (100–300 km). Durations predicted for small events (M_w < 5) by this model and the AS16 model are systematically higher than the KS06 and BSA09 models. This is not surprising because the database used in KS06 and BSA09 contains a very limited number of small-magnitude recordings. The predictive trends of the KS06 and BSA09 models at the small-magnitude range may not be properly constrained by the database used. It has been reported that the GMPEs based on the NGA-West1 database (e.g., Boore and Atkinson, 2008; Campbell and Bozorgnia, 2008) generally overpredict the PGA values for small-magnitude events (Boore *et al.*, 2014; Campbell and Bozorgnia, 2014). Considering the fact that Ds are negatively correlated with PGA (Bradley, 2011), the existing models using the NGA-West1 database tend to underpredict Ds for small-magnitude earthquakes. Therefore, the proposed model can better estimate significant durations at the small-magnitude range.

Figure 11 compares the total standard deviations σ and σ_{ARB} from this study with those from the other three models. As can be seen from these plots, although a magnitude-dependent variability model is adopted in this study, the total standard deviations of these models are generally in a similar range. Both this study and the AS16 model indicate that the standard deviations for smaller magnitude events are generally larger than those of larger events.

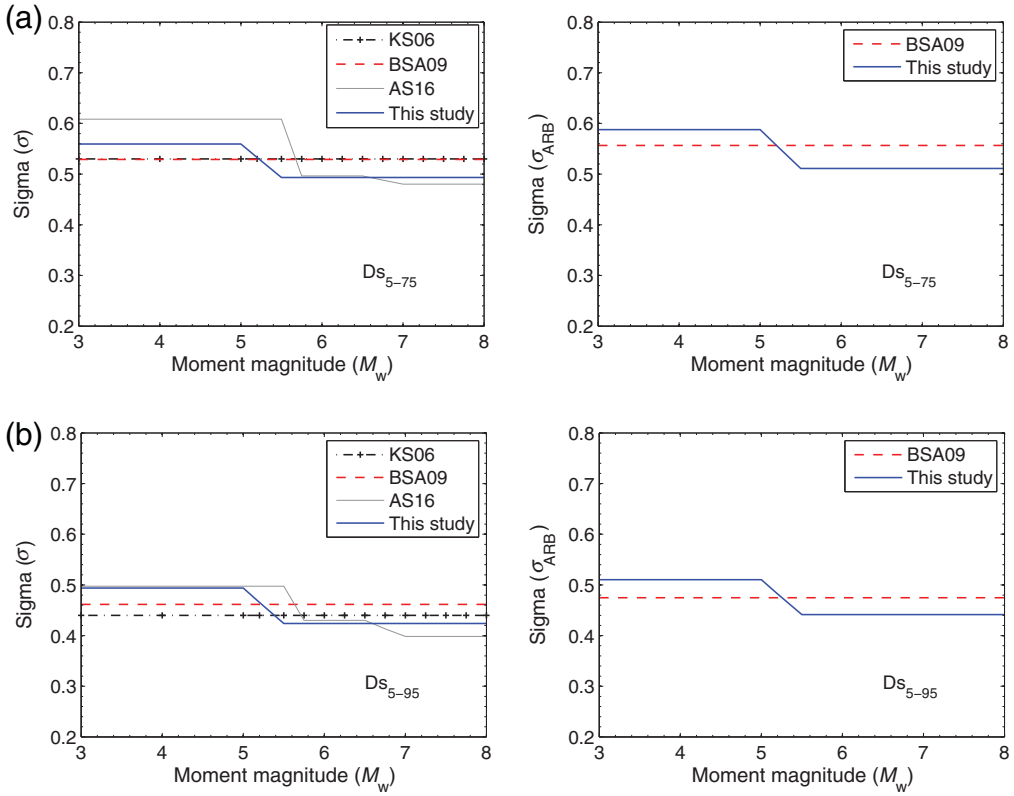

Figure 11. Comparisons of the total standard deviations (geometric mean component σ and arbitrary component σ_{ARB}) from this study with the other predictive models for (a) $\mathrm{Ds}_{5\text{–}75}$ and (b) $\mathrm{Ds}_{5\text{–}95}$. Note that the component-to-component variability ϕ_c was not specified in the Kempton and Stewart (2006; KS06) and Afshari and Stewart (2016; AS16) models. The color version of this figure is available only in the electronic edition.

Empirical Correlation Analysis

Empirical correlations between ground-motion IMs are important in seismic-hazard analysis and the ground-motion selection process. Some researchers have studied the empirical correlations between various IMs (e.g., Baker and Jayaram, 2008; Bradley, 2011; Wang and Du, 2012, 2013; Huang and Wang, 2015). Specifically, Bradley (2011) has developed parametric equations to quantify the correlations between significant durations and other IMs, using the ground motions selected in the NGA-West1 database. It is tempting to further examine the empirical correlations between significant durations and other IMs such as PGA, peak ground velocity (PGV), and SA using the NGA-West2 database.

Similar to equation (2), current GMPEs usually assume that IMs are normally distributed in logarithmic scale, which can be shown as

$$\ln(\mathrm{IM}_k) = \overline{\ln(\mathrm{IM}_k)} + \eta_k + \varepsilon_k, \tag{12}$$

in which $\ln(\mathrm{IM}_k)$ and $\overline{\ln(\mathrm{IM}_k)}$ denote the measured and the predicted logarithmic kth IM, respectively. η_k and ε_k represent the between-event and within-event residuals for the kth IM. Statistical tests have been performed to prove the normality of the between-event and within-event residuals associated with SA (Jayaram and Baker, 2008). The correlation coefficients between the between-event and within-event residuals for different IMs can be estimated using the well-known Pearson product-moment correlation estimator

$$\rho_{x_1,x_2} = \frac{\sum_{i=1}^{n}(x_1^{(i)} - \overline{x_1})(x_2^{(i)} - \overline{x_2})}{\sqrt{\sum_{i=1}^{n}(x_1^{(i)} - \overline{x_1})^2 \sum_{j=1}^{n}(x_2^{(j)} - \overline{x_2})^2}} \tag{13}$$

(Ang and Tang, 2007), in which x_1 and x_2 are random variables; n is the total number of the considered random variables; $\overline{x_1}$ and $\overline{x_2}$ denote the sample mean of variables x_1 and x_2, respectively. Therefore, ρ_{η_1,η_2} and $\rho_{\varepsilon_1,\varepsilon_2}$ representing the correlations of between-event and within-event residuals between IM_1 and IM_2 can be estimated via equation (13). In this study, IM_1 refers to Ds and IM_2 refers to PGA, PGV, and SA at different periods. For demonstration purpose, Figure 12a shows the scatter plot of the within-event residuals for $\mathrm{Ds}_{5\text{–}75}$ and PGA. The corresponding correlation coefficient obtained by equation (13) is −0.51.

Under the assumptions that the between-event and within-event residuals of IMs are independent (Abrahamson and Youngs, 1992), the correlation between the total residuals ρ_{T_1,T_2} can be expressed as a combination of the between-event and within-event correlations as

$$\rho_{T_1,T_2} = \frac{1}{\sigma_1 \times \sigma_2}(\rho_{\eta_1,\eta_2}\tau_1\tau_2 + \rho_{\varepsilon_1,\varepsilon_2}\phi_1\phi_2) \tag{14}$$

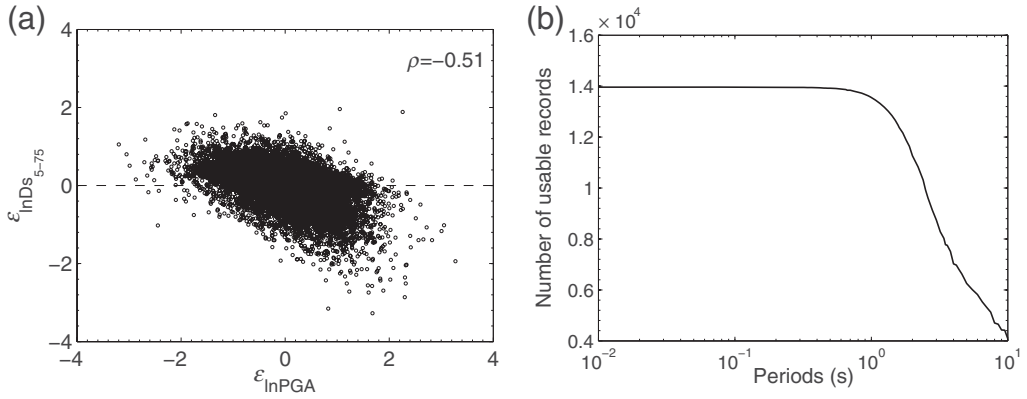

Figure 12. (a) Distribution of within-event residuals illustrating negative correlation between Ds_{5-75} and peak ground acceleration (PGA). (b) Number of usable records to compute the correlation of significant durations with spectral acceleration (SA) at different periods.

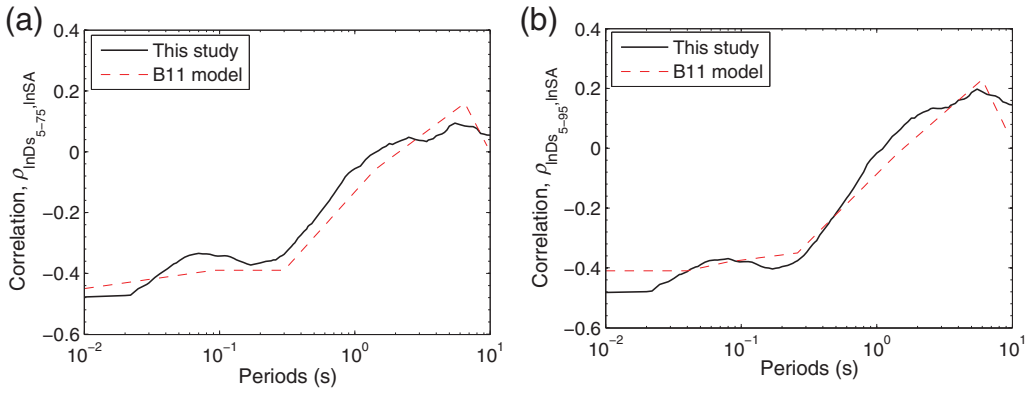

Figure 13. Empirical correlations between significant durations and SA at various periods: (a) Ds_{5-75}–SA and (b) Ds_{5-95}–SA. The parametric equations proposed by Bradley (2011) are also plotted for comparison. The color version of this figure is available only in the electronic edition.

(Bradley, 2011), in which τ_k, φ_k, and σ_k ($k = 1, 2$) are the standard deviations of the between-event, within-event, and total residuals for the kth IM, respectively. For each pair of IMs, the correlation between the total residuals can be calculated via equations (13) and (14).

To compute the Ds–SA correlations, the predicted median SA and standard deviations at each period are computed using the Campbell–Bozorgnia NGA-West2 model (Campbell and Bozorgnia, 2014, hereafter CB14). It should be noted that each recorded time history has a usable frequency range which is related to removing low- or high-frequency noises in signal processing. Thus, only SA for periods less than the inverse of the lowest usable frequency is used to compute the Ds–SA correlation coefficients. The number of usable records is then expected to decrease as the vibration period increases, as shown in Figure 12b.

Once the predicted median SAs of the CB14 model for each recording are computed, the total SA residuals can be calculated. Based on the provided τ_{SA}, ϕ_{SA}, and σ_{SA} (between-event, within-event, and total aleatory standard deviations) of the CB14 model, the total SA residuals can be partitioned into between-event and within-event residuals by performing the random-effects regression (Abrahamson and Youngs, 1992). Then, the correlations between the between-event and within-event residuals for Ds and SA can be computed. Finally, equation (14) can be used to calculate the correlations between the total residuals of Ds and SA.

Figure 13a and 13b shows the computed empirical correlations for Ds_{5-75}–SA and Ds_{5-95}–SA, respectively. It is shown that the correlation coefficients between Ds and SA at periods smaller than about 1.2 s are negative, and the negative correlation becomes weaker as the spectral period increases. The piecewise linear fitting equations (termed as the B11 model) proposed by Bradley (2011) are also shown in these plots for comparison. Results from this study are, in general, consistent with the B11 model predictions. Table 4 shows the computed empirical correlations between Ds_{5-75}, Ds_{5-95}, PGA, and PGV, respectively, with values from Bradley (2011) in parenthesis for comparison. Again, these computed correlations are generally consistent with those presented by Bradley (2011). The study implies that although the NGA-West1 database includes a much smaller number of ground motions, it still can be used reliably to compute the empirical correlations between different IMs.

Table 4
Estimated Correlation Coefficients of $Ds_{5–75}$ and $Ds_{5–95}$ with Peak Ground Acceleration (PGA) and Peak Ground Velocity (PGV), with Values from Bradley (2011) in Parenthesis for Comparison

	PGA	PGV	$Ds_{5–95}$
$Ds_{5–75}$	−0.47 (−0.44)	−0.39 (−0.26)	0.82 (0.84)
$Ds_{5–95}$	−0.48 (−0.41)	−0.35 (−0.21)	—

Conclusions

This study presented new prediction equations for significant durations $Ds_{5–75}$ and $Ds_{5–95}$, using 13,958 well-recorded ground motions selected from the latest NGA-West2 database. The equations are expressed as a function of moment magnitude (M_w), rupture distance (R_{rup}), site parameter (V_{S30}), and depth to the top of the fault rupture (Z_{tor}). The proposed model can be applied to shallow crustal earthquakes with moment magnitude ranging from 3 to 7.9, and rupture distance less than 300 km.

It was observed that the variability of the within-event residuals for $M_w < 5$ is larger than that for $M_w > 5.5$. Similar to the NGA-West2 GMPEs, a magnitude-dependent within-event standard deviation structure is proposed. Compared with a constant standard deviation model, the proposed tri-linear model can better predict the aleatory variability of various earthquake scenarios.

The performance of the new model has been compared with three other predictive models that were developed based on the NGA database. The predictions of significant durations for earthquakes with moderate-to-large magnitude ($M_w \geq 5$) and $R_{rup} \leq 100$ km are generally consistent. However, compared with the models developed based on the NGA-West1 database, noticeable discrepancies can be observed for scenarios with small magnitudes ($M_w < 5.5$). This is expected, because the NGA-West2 database is abundant in small-to-moderate events. Therefore, the new model can reasonably improve the estimates of Ds for small-magnitude or far-source earthquake scenarios, owing to the use of the expanded database. We do not think that the new model is definitely superior to the other models, but rather provides an interpretation of the latest database.

Finally, the empirical correlations between Ds and other IMs such as PGA and SA were investigated. It was found that the empirical correlations using the NGA-West2 database are generally consistent with previous studies using the NGA-West1 database. Therefore, the empirical correlations are relatively insensitive to the selection of ground-motion database. We recommend the parametric Ds–SA correlation models proposed by Bradley (2011) for practical applications.

Data and Resources

Ground-motion time histories used in this study are obtained from the Pacific Earthquake Engineering Research (PEER) Next Generation Attenuation (NGA) database (http://ngawest2.berkeley.edu/, last accessed August 2015). The NGA-West2 database flatfile including source, site information as well as rupture distances are downloaded via http://peer.berkeley.edu/ngawest2/databases/ (last accessed August 2015).

Acknowledgments

The work described in this article was supported by Hong Kong Research Grants Council through General Research Fund Grant Number 16213615 and Collaborative Research Fund Grant Number CityU8/CRF/13G. The authors thank the Pacific Earthquake Engineering Research (PEER) researchers who compiled the Next Generation Attenuation-West2 (NGA-West2) ground-motion database and make it available to the public. The authors thank two anonymous reviewers and Associate Editor Peter Stafford for their helpful comments to improve this article.

References

Abrahamson, N. A., and W. J. Silva (1996). Empirical ground motion models, *Report to Brookhaven National Laboratory*, New York, New York.

Abrahamson, N. A., and R. R. Youngs (1992). A stable algorithm for regression analysis using the random effects model, *Bull. Seismol. Soc. Am.* **82,** no. 1, 505–510.

Abrahamson, N. A., W. J. Silva, and R. Kamai (2014). Summary of the ASK14 ground motion relation for active crustal regions, *Earthq. Spectra* **30,** no. 3, 1025–1055.

Afshari, K., and J. P. Stewart (2016). Physically parameterized prediction equations for significant duration in active crustal regions, *Earthq. Spectra* **32,** no. 4, 2057–2081.

Al Atik, L., N. Abrahamson, J. J. Bommer, F. Scherbaum, F. Cotton, and N. Kuehn (2010). The variability of ground-motion prediction models and its components, *Seismol. Res. Lett.* **81,** no. 5, 794–801.

Allmann, B. P., and P. M. Shearer (2009). Global variations of stress drop for moderate to large earthquakes, *J. Geophys. Res.* **114,** no. B01310, doi: 10.1029/2008JB005821.

Ancheta, T. D., R. B. Darragh, J. P. Stewart, E. Seyhan, W. J. Silva, B. S. J. Chiou, and J. L. Donahue (2014). NGA-West2 database, *Earthq. Spectra* **30,** no. 3, 989–1005.

Ang, A. H. S., and W. H. Tang (2007). *Probability Concepts in Engineering: Emphasis on Applications in Civil and Environmental Engineering*, John Wiley & Sons, New York, New York.

Arias, A. (1970). A measure of earthquake intensity, in *Seismic Design for Nuclear Power Plants*, R. J. Hansen (Editor), MIT Press, Cambridge, Massachusetts, 438–483.

Baker, J. W., and C. A. Cornell (2006). Which spectral acceleration are you using?, *Earthq. Spectra* **22,** 293–312.

Baker, J. W., and N. Jayaram (2008). Correlation of spectral acceleration values from NGA ground motion models, *Earthq. Spectra* **24,** no. 1, 299–317.

Bommer, J. J., and A. Martinez-Pereira (1999). The effective duration of earthquake strong motion, *J. Earthq. Eng.* **3,** no. 2, 127–172.

Bommer, J. J., G. Magenes, J. Hancock, and P. Penazzo (2004). The influence of strong-motion duration on the seismic response of masonry structures, *Bull. Earthq. Eng.* **2,** no. 1, 1–26.

Bommer, J. J., P. J. Stafford, and J. A. Alarcón (2009). Empirical equations for the prediction of the significant, bracketed, and uniform duration of earthquake ground motion, *Bull. Seismol. Soc. Am.* **99,** no. 6, 3217–3233.

Boore, D. M. (1983). Stochastic simulation of high-frequency ground motions based on seismological models of the radiated spectra, *Bull. Seismol. Soc. Am.* **73,** no. 6A, 1865–1894.

Boore, D. M. (2005). Erratum: Equations for estimating horizontal response spectra and peak acceleration from western North American earthquakes: A summary of recent work, *Seismol. Res. Lett.* **76,** 368–369.

Boore, D. M., and G. M. Atkinson (2008). Ground-motion prediction equations for the average horizontal component of PGA, PGV, and 5%-damped PSA at spectral periods between 0.01 s and 10.0 s, *Earthq. Spectra* **24,** no. 1, 99–138.

Boore, D. M., and E. M. Thompson (2014). Path durations for use in the stochastic-method simulation of ground motions, *Bull. Seismol. Soc. Am.* **104,** no. 5, 2541–2552.

Boore, D. M., J. P. Stewart, E. Seyhan, and G. M. Atkinson (2014). NGA-West2 equations for predicting PGA, PGV, and 5% damped PSA for shallow crustal earthquakes, *Earthq. Spectra* **30,** no. 3, 1057–1085.

Bora, S. S., F. Scherbaum, N. Kuehn, and P. J. Stafford (2014). Fourier spectral and duration models for the generation of response spectra which are adjustable to different source-, propagation-, and site effects, *Bull. Earthq. Eng.* **12,** no. 3, 467–493.

Bora, S. S., F. Scherbaum, N. Kuehn, P. Stafford, and B. Edwards (2015). Development of a response spectral ground-motion prediction equation (GMPE) for seismic hazard analysis from empirical Fourier spectral and duration models, *Bull. Seismol. Soc. Am.* **105,** no. 4, 2192–2218.

Bradley, B. A. (2011). Correlation of significant duration with amplitude and cumulative intensity measures and its use in ground motion selection, *J. Earthq. Eng.* **15,** no. 6, 809–832.

Brune, J. N. (1970). Tectonic stress and the spectra of seismic shear waves from earthquakes, *J. Geophys. Res.* **75,** no. 26, 4997–5009.

Campbell, K. W., and Y. Bozorgnia (2008). NGA ground motion model for the geometric mean horizontal component of PGA, PGV, PGD and 5% damped linear elastic response spectra for periods ranging from 0.1 to 10 s, *Earthq. Spectra* **24,** no. 1, 139–171.

Campbell, K. W., and Y. Bozorgnia (2013). NGA-West2 Campbell–Bozorgnia ground motion model for the horizontal components of PGA, PGV, and 5%-damped elastic pseudo-acceleration response spectra for periods ranging from 0.01 to 10 s, *PEER Report No. 2013/06*, Pacific Earthquake Engineering Research Center, University of California, Berkeley, California, 238 pp.

Campbell, K. W., and Y. Bozorgnia (2014). NGA-West2 ground motion model for the average horizontal components of PGA, PGV, and 5% damped linear acceleration response spectra, *Earthq. Spectra* **30,** no. 3, 1087–1115.

Chandramohan, R., J. W. Baker, and G. G. Deierlein (2016). Quantifying the influence of ground motion duration on structural collapse capacity using spectrally equivalent records, *Earthq. Spectra* **32,** no. 2, 927–950.

Chiou, B. S. J., and R. R. Youngs (2014). Update of the Chiou and Youngs NGA model for the average horizontal component of peak ground motion and response spectra, *Earthq. Spectra* **30,** no. 3, 1117–1153.

Chiou, B., R. Darragh, N. Gregor, and W. Silva (2008). NGA project strong-motion database, *Earthq. Spectra* **24,** no. 1, 23–44.

Dobry, R., I. M. Idriss, and E. Ng (1978). Duration characteristics of horizontal components of strong-motion earthquake records, *Bull. Seismol. Soc. Am.* **68,** no. 5, 1487–1520.

Du, W., and G. Wang (2013). A simple ground-motion prediction model for cumulative absolute velocity and model validation, *Earthq. Eng. Struct. Dynam.* **42,** no. 8, 1189–1202.

Foulser-Piggott, R., and P. J. Stafford (2012). A predictive model for Arias intensity at multiple sites and consideration of spatial correlations, *Earthq. Eng. Struct. Dynam.* **41,** no. 3, 431–451.

Ghofrani, H., and G. M. Atkinson (2015). Duration of the 2011 Tohoku earthquake ground motions, *J. Seismol.* **19,** no. 1, 9–25.

Green, R. A., and G. A. Terri (2005). Number of equivalent cycles concept for liquefaction evaluations—Revisited, *J. Geotech. Geoenviron. Eng.* **131,** no. 4, 477–488.

Hancock, J., and J. J. Bommer (2006). A state-of-knowledge review of the influence of strong-motion duration on structural damage, *Earthq. Spectra* **22,** no. 3, 827–845.

Hancock, J., and J. J. Bommer (2007). Using spectral matched records to explore the influence of strong-motion duration on inelastic structural response, *Soil Dynam. Earthq. Eng.* **27,** no. 4, 291–299.

Hanks, T. C., and R. K. McGuire (1981). The character of high-frequency strong ground motion, *Bull. Seismol. Soc. Am.* **71,** no. 6, 2071–2095.

Hernandez, B., and F. Cotton (2000). Empirical determination of the ground shaking duration due to an earthquake using strong motion accelerograms for engineering applications, *Proc. of 12th World Conf. on Earthquake Engineering*, Paper No. 2254/4.

Huang, D., and G. Wang (2015). Region-specific spatial cross-correlation model for regionalized stochastic simulation of ground-motion time histories, *Bull. Seismol. Soc. Am.* **105,** no. 1, 272–284.

Idriss, I. M., and R. W. Boulanger (2006). Semi-empirical procedures for evaluating liquefaction potential during earthquakes, *Soil Dynam. Earthq. Eng.* **26,** no. 2, 115–130.

Iervolino, I., G. Manfredi, and E. Cosenza (2006). Ground motion duration effects on nonlinear seismic response, *Earthq. Eng. Struct. Dynam.* **35,** no. 1, 21–38.

Jayaram, N., and J. W. Baker (2008). Statistical tests of the joint distribution of spectral acceleration values, *Bull. Seismol. Soc. Am.* **98,** no. 5, 2231–2243.

Kagawa, T., K. Irikura, and P. G. Somerville (2004). Differences in ground motion and fault rupture process between the surface and buried rupture earthquakes, *Earth Planets Space* **56,** no. 1, 3–14.

Kaklamanos, J., L. G. Baise, and D. M. Boore (2011). Estimating unknown input parameters when implementing the NGA ground-motion prediction equations in engineering practice, *Earthq. Spectra* **27,** no. 4, 1219–1235.

Kempton, J. J., and J. P. Stewart (2006). Prediction equations for significant duration of earthquake ground motions considering site and near-source effects, *Earthq. Spectra* **22,** no. 4, 985–1013.

Lee, J., and R. A. Green (2014). An empirical significant duration relationship for stable continental regions, *Bull. Earthq. Eng.* **12,** no. 1, 217–235.

Pinheiro, J., D. Bates, S. DebRoy, D. Sarkar, and R Core Team (2008). *NLME: Linear and Nonlinear Mixed Effects Models*, R Package Version 3, 1–89.

Reinoso, E., and M. Ordaz (2001). Duration of strong ground motion during Mexican earthquakes in terms of magnitude, distance to the rupture area and dominant site period, *Earthq. Eng. Struct. Dynam.* **30,** no. 5, 653–673.

Seed, H. B., and K. L. Lee (1966). Liquefaction of saturated sands during cyclic loading, *J. Soil Mech. Found. Div.* **92,** no. 6, 105–134.

Trifunac, M. D., and A. G. Brady (1975). A study on the duration of strong earthquake ground motion, *Bull. Seismol. Soc. Am.* **65,** no. 3, 581–626.

Wang, G., and W. Du (2012). Empirical correlations between cumulative absolute velocity and spectral accelerations from NGA ground motion database, *Soil Dynam. Earthq. Eng.* **43,** 229–236.

Wang, G., and W. Du (2013). Spatial cross-correlation models for vector intensity measures (PGA, I_a, PGV, and SAs) considering regional site conditions, *Bull. Seismol. Soc. Am.* **103,** no. 6, 3189–3204.

Yaghmaei-Sabegh, S., Z. Shoghian, and M. N. Sheikh (2014). A new model for the prediction of earthquake ground-motion duration in Iran, *Nat. Hazards* **70,** no. 1, 69–92.

Institute of Catastrophe Risk Management
Nanyang Technological University
50 Nanyang Avenue, North Spine, Block N1-B1b-08
Singapore 639798, Singapore
wqdu@ntu.edu.sg
(W.D.)

Department of Civil and Environmental Engineering
The Hong Kong University of Science and Technology
Room 3594, Academic Building
Clear Water Bay, Hong Kong
gwang@ust.hk
(G.W.)

Manuscript received 3 December 2015;
Published Online 27 December 2016